

Comparative Microstructural Analysis of Nongraphitic Carbons by Wide-Angle X-ray and Neutron Scattering

Torben Pfaff,^{†,‡} Felix M. Badaczewski,^{†,‡} Marc O. Loeh,^{†,‡} Alexandra Franz,[§] Jens-Uwe Hoffmann,[§] Manfred Reehuis,[§] Wolfgang G. Zeier,^{†,||} and Bernd M. Smarsly*,^{†,‡,||}

[†]Institute of Physical Chemistry, Justus Liebig University, Heinrich-Buff-Ring 17, D-35392 Giessen, Germany

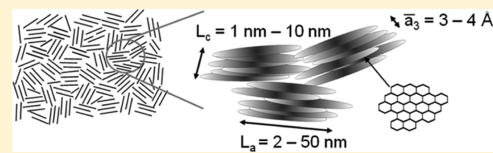
[‡]Schunk Carbon Technology, Schunk GmbH, D-35452 Heuchelheim, Germany

[§]Helmholtz Zentrum Berlin für Materialien und Energie, D-14109 Berlin, Germany

^{||}Center for Materials Research (LaMa), Justus Liebig University, Heinrich-Buff-Ring 16, D-35392 Giessen, Germany

S Supporting Information

ABSTRACT: Non-graphitic carbons (NGCs) represent the most abundant class of sp^2 -hybridized carbon materials (coal char coal, activated carbon, etc.). These carbons consist of small graphene layer stacks possessing significant structural disorder in both the single graphene sheets and the stacking. In this study an advanced evaluation approach for wide-angle neutron scattering (WANS) was developed, based on the method introduced by Ruland and Smarsly in 2002. In particular, we elucidated if and how the enhanced WANS data quality and larger values of the modulus of the scattering vector s -range affect the accuracy and the values of the size and disorder parameters—being fitting parameters by themselves—in comparison to wide-angle X-ray scattering (WAXS), which is usually performed by laboratory equipment. We find a reasonable agreement for the parameters L_a and L_c , that is, the lateral dimension and stack height, within the error bars, whereas for the disorder parameters different results for WAXS and WANS were found, the origin of which is discussed. Thus, this study addresses the general issue of how reliably microstructural parameters can be determined from WAXS/WANS by fitting simulated WAXS and WANS curves, which are quality-impaired by added Gaussian noise at different levels and cut-off at different s -values. From this analysis, we estimated the minimal data quality required for a reliable NGC microstructural analysis based on WAXS/WANS. As an important finding, these simulations show that typical, standard WAXS laboratory setups are sufficient to provide reliable values for the most relevant structural parameters. Furthermore, pair-distribution function (PDF) analyses were performed on WAXS data obtained from a synchrotron facility. Comparing PDF and WAXS/WANS fitting analysis suggests the presence of small highly ordered oligoaromatic domains embedded in the larger graphene sheets, questioning the classical view on the NGC microstructure.



INTRODUCTION

Carbon occurs in many forms, of which diamond (made up of sp^3 -hybridized carbon) and graphite (made up of sp^2 -hybridized carbon) are the most common ones. Among the sp^2 -hybridized carbons the so-called “non-graphitic carbons (NGCs)”, a million-ton-scale class of materials, are of significant relevance for applications in both academia and industry and comprise a plurality of carbons such as activated carbon, glassy carbon, carbide-derived carbon, and so forth. NGCs consist of graphene stacks, which typically possess nanometer dimensions and, as major structural feature, rotational and translational disorder,¹ that is a “turbostratic” arrangement. This absence of long-range crystallographic order causes broad and overlapping scattering maxima in wide-angle X-ray scattering (WAXS) and wide-angle neutron scattering (WANS), which also constitutes the definition of NGCs by IUPAC.² The general structure of NGCs is depicted in Figure 1. The main structural dimensions of these stacks are generally described by the parameters L_a and L_c , which are the average lateral extension and stack height, respectively. Further important and relevant parameters are the C–C bond length,

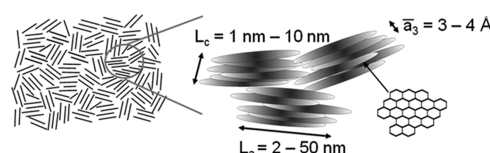


Figure 1. Basic structure of NGCs. NGCs consist of a turbostratic arrangement of parallel sp^2 -layers. This figure is adapted from (ref 3).

l_{CC} , the average distance between the layers, \bar{a}_3 , and also parameters quantifying the substantial degree of disorder in the stacking (σ_3) and the layers themselves (σ_1).

NGCs have a broad scope of application: pitch-based NGCs are used as material for electrodes in batteries, carbide-derived carbons in supercapacitors, and activated carbon for filters and molecular sieves. Hence, a quantitative determination of the aforementioned microstructure based on experimentally accessible structural parameters is crucial for a fundamental

Received: April 16, 2019

Revised: July 7, 2019

Published: July 9, 2019

understanding of the linkage between material properties and the microstructure. Relevant macroscopic properties like hardness, chemical stability, or thermal and electrical conductivity are, at least in part, determined by the microstructure on the Ångstrom and nanometer scale. For example, Krüner et al. found that higher synthesis temperatures and the presence of ammonia lead to a more ordered nongraphitic structure of nitrogen-containing novolac-derived carbon beads.⁴ Electrochemical characterization of these materials revealed that their capacity and specific surface area increase with increasing degree of order of the graphene stacks. The correlation between mesopore size and degree of order has also been reported by Badaczewski et al.⁵

Three main approaches are usually applied for the microstructural analysis of NGCs, which are WAXS, transmission electron microscopy (TEM), and Raman scattering. Among them, WAXS offers fundamental advantages, in particular the straightforward experimental analysis using standard X-ray powder diffraction lab setups. Raman scattering is used as the standard characterization for NGCs, providing the L_a value, but especially for small graphene dimensions the currently used analyses still need verification by an independent approach, for example by WAXS or WANS. The most distinct features of WAXS data of NGCs are the superposition of the scattering from the single graphenes ("intralayer scattering") and their stacking ("interlayer scattering"), as well as the large width of the maxima. The width of the interlayer and intralayer reflections is determined by both size and disorder, and it is thus the task of any evaluation approach to separate these two structural features. However, owing to the broad and overlapping WAXS reflections, evaluation approaches based on analyzing the width of individual WAXS/WANS reflections are inappropriate for the microstructural analysis of NGCs. In contrast, it is recommendable to fit the entire WAXS curve using a suitable theoretical model function. The first such approach was proposed by Shi et al. in 1993,⁶ followed by other approaches by Azuma in 1998⁷ as well as Fujimoto and Shiraishi in 2001.⁸ In 2002 Ruland & Smarsly published an approach for the evaluation of the WAXS of NGCs⁹ that has already been successfully used in several studies^{10–13} and incorporated in CarbX,¹⁴ an "easy-to-use" software for microstructural analysis of NGCs based on WAXS. A main objective of the Ruland and Smarsly model is the quantification of the dimension of the graphene stacks as well as the disorder in the graphenes themselves and in their stacking, by separating the effects of size and disorder, which both determine the widths of the reflections. Very recently, also Puech et al. proposed an approach, which utilizes the fitting of entire WAXS data.¹⁵

Whereas the approach of Ruland and Smarsly provides meaningful structural characterization of NGCs, the analysis of NGCs by WAXS and thus the validity of the aforementioned approaches generally suffer from the following features: First, atomic form factors result in the damping of WAXS maxima at large values of the modulus of the scattering vector. Second, the Compton scattering has to be exactly taken into account, which is more pronounced at larger scattering vectors as well. Third, the limited range of the modulus of the maximum scattering vector available in widespread lab X-ray diffraction (XRD) setups limits the number of accessible WAXS reflections. Using the averaged Cu-K α wavelength of 1.5418 Å, WAXS data of typical NGCs might show only a handful reflections. A large number of reflections is, however, crucial to

distinguish between size (L_a & L_c) and disorder effects (σ_1 & σ_3), which both influence the significant width of the reflections. This dilemma is therefore inherent to nanostructured materials, in which the width of WAXS/WANS reflections is influenced by two phenomena, finite size, and structural disorder.

In essence, the accessibility of larger scattering vectors thus might allow for a more profound understanding of disorder on the level of small graphene units. As WANS usually offers a much wider range of scattering vectors, is based on constant coherent neutron scattering lengths, and does not suffer from the impact of Compton scattering, it provides fundamental advantages compared to lab WAXS setups. As a complementary technique, special setups enable the analysis of WAXS and WANS data at very large scattering vectors $s = \frac{2\sin(\theta)}{\lambda}$, from which the so-called pair distribution function (PDF) can be obtained, which is mostly used to determine bond-lengths.

Despite its advantages, WANS has been scarcely used for the microstructural analysis of NGCs. In 2005, Burian et al. acquired WANS data of activated carbons, drawing qualitative conclusions therefrom.¹⁶ In 2006, Prem et al. utilized WANS to analyze carbon/carbon composite materials.¹⁷ They extracted the L_a and L_c values from WANS data using the full width at half-maximum (FWHM) of the first interlayer and intralayer reflections, respectively. In 2012, Weisbecker et al. used a PDF analysis based on neutron diffraction data to elucidate the microstructure of pyrocarbons.¹⁸ Here, X-ray diffraction and the Scherrer equation were used for extraction of L_a & L_c as well as atomistic modeling to simulate PDF patterns. The results of the PDF analysis corresponded well to complementary methods like TEM and Raman spectroscopy. In a followup study¹⁹ the L_a and L_c values were obtained from the (10) and (002) reflections of the total neutron diffraction structure factors derived from WANS data. Again, good agreement between results derived from neutron diffraction and complementary experimental (quantitative TEM image analysis) and theoretical (atomistic modeling) analysis methods was found. PDF analysis of neutron diffraction data was used in two further studies by Woznica et al. in 2015 and Jurkiewicz et al. in 2017. Woznica et al. investigated a material consisting of three layers of graphene and concluded that the material is best described using a paracrystalline model both to describe disorder within the layers and stacking of the layers.²⁰ The study of Jurkiewicz et al. focused on glass-like carbons derived from furfuryl alcohol and proposed a new model to describe their structure.²¹ In this model, the structure is considered to be made up of curved sp² planes, and the curvature emerges from the presence of non-six-member rings and agglomerated point defects. Besides simulation of and comparison with experimental PDF patterns, the C–C bond length and valence angle were extracted from the model used. In summary, both studies used distinct structure models to simulate scattering data and verified those by good agreement between experimental and simulated data.

In spite of these studies, including our own contributions, we believe that an important, fundamental question in the structure of NGCs has not been sufficiently addressed: the degree of structural disorder in carbons with small graphene extension (i.e., small L_a and L_c) is still a matter of debate. To be more specific, it has not been clarified yet, if indeed "disordered" NGCs possess a heavily disarranged polycyclic structure (as proposed by large values of parameters describing

the disorder (σ_1 & σ_3) determined by WAXS), or if the limited accessible data range impedes an accurate separation of the disorder from the broad scattering maxima. In essence, a major goal of this study therefore was to determine how far from perfect graphite the graphene structure of NGCs is.

However, in the aforementioned WANS studies merely a few microstructural parameters were derived, for example the C–C bond length from PDF analysis, L_a and L_c values. Consequently, in the present study we pursue a comprehensive methodology to address, on the basis of WAXS and WANS evaluation, the following fundamental questions:

- To which extent are the values of the most relevant structural parameters (i.e., L_a , L_c , σ_1 , σ_3) affected by typical shortcomings of powder WAXS lab analysis (cutoff and atomic form factor)?
- Can parameters describing size (L_a , L_c) and disorder (σ_1 , σ_3 , see the approach of Ruland and Smarsly) be accurately separated from the width of WAXS/WANS reflections?
- Is a meaningful, precise characterization of the structure of NGCs possible by standard WAXS setups?
- How disordered are “disordered” NGCs, in relation to graphite, and what is the nature of this disorder?

To approach these items, the present study uses the following strategy:

1. We adapted Ruland and Smarsly's approach for the evaluation of WANS data, which requires only few modifications to the original WAXS approach with respect to the form factor and Compton scattering (see section [WAXS and WANS of NGC](#)). The applicability of Ruland and Smarsly's model for WANS was tested by analyzing WANS data of several NGCs.
2. Using the Ruland/Smarsly model adapted to WANS, we elucidated if and how the enhanced WANS data quality and larger s -range (discussed in the section [WANS and WAXS Data](#)) affect the accuracy and the values of the size and disorder parameters—being fitting parameters by themselves—in comparison with WAXS (see section [WAXS/WANS Comparison](#)).
3. On the issue of how reliably the originary microstructure can be reconstructed from WAXS/WANS data, the error range of the parameters obtained by WANS and WAXS was studied in a separate set of analyses (see the section [Simulated Data](#)). Our previous study indicated that this uncertainty (error bar) in the values was relatively large¹² and thus reduces the validity of the obtained parameters. In order to approach the magnitude of uncertainty in a systematic way, we simulated WAXS and WANS data, using the Ruland and Smarsly approach, having different s -ranges and artificial noise levels, which were then analyzed by the Ruland and Smarsly approach as “experimental” data. By comparing the original structural parameters with those obtained from the evaluation, the minimal data quality (in terms of noise and available s -range) which is required for a precise and reliable quantification of the microstructural parameters was determined. Furthermore, such simulation “experiments” indicated how reliably the originary microstructure can be reconstructed based on the Ruland and Smarsly approach and scattering methods in general.

4. In order to determine the degree of disorder in NGCs on a local scale by an independent method, PDF analysis was carried out on suitable WAXS data obtained from a synchrotron facility. Such analysis can provide the mutual alignment of benzene rings and bond lengths within them. Obviously, both precise and accurate parameters are crucial, and a large s -range is required; therefore, the data were acquired at a synchrotron beamline with an appropriate setup for obtaining high-quality PDF. The main focus of the PDF analysis was to compare the width of the PDF signal maxima to those of graphite in order to determine the degree of disorder within the smallest building units of NGCs. Also, by comparing and combining the results of PDF and WANS data analysis, the values and in particular the nature of the structural disorder were determined (see section [PDF Analysis](#)).

In conclusion, the present study focusses on specific, yet quite important aspects in the appropriate analysis of WAXS/WANS data of carbon materials, which in turn provides the basis for a valid quantitative characterization of this class of materials in general.

EXPERIMENTAL AND THEORETICAL METHODS

In this section, first the model used to fit NGC WANS data is described in the subsection [WAXS and WANS of NGC](#). Second, in the subsection [Experimental Methods](#) our experimental methods are presented.

WAXS and WANS of NGC. To fit WANS data of NGCs a modified version of Ruland & Smarsly's algorithm described in refs^{9,12–14} was used, which was developed for the evaluation of WAXS of NGCs. In the following, we summarize the algorithm used to model NGC WAXS data, and the modification of this approach to analyze WANS data is given afterwards.

The theoretically observable scattering intensity $I_{\text{theoretical}}$ is proportional to the sum of coherent scattering I_{coh} and incoherent scattering I_{incoh} :

$$I_{\text{theoretical}} \propto (I_{\text{coh}} + I_{\text{incoh}}) \quad (1)$$

The coherent scattering intensity arises from scattering by the layers themselves (intralayer scattering), producing (hk) reflections, and scattering from the stacking of the layers (interlayer scattering), producing $(00l)$ reflections. It is assumed that there is no 3D correlation between the stacked graphenes. The principal idea of this superposition of scattering intensities is depicted in [Figure 2](#), showing the asymmetric (hk) intralayer and symmetric $(00l)$ interlayer reflections. In particular, the pronounced overlapping of the broad reflections impedes analysis of single maxima. Hence, our approach of fitting the entire WAXS/WANS curve is favorable.

Expressions for the scattering of the layers were already developed by ref 1 and further developed recently, see ref 9. Further contributions are scattering from unorganized carbon c_{un} , nitrogen c_{N} , and oxygen c_{O} impurities. These modifications hold true for both, WAXS and WANS. In addition, the anisotropy of the atomic scattering factor (WAXS) for carbon perpendicular to the graphene sheets $f_{\text{C},\text{perp}}$ has to be considered. The slight change of the tabulated form factor for carbon caused by this anisotropy is accounted for by the empirical parameter Δ_{an} which is used for the calculation of $f_{\text{C},\text{perp}}$ (please refer to the Supporting Information of ref 14 for

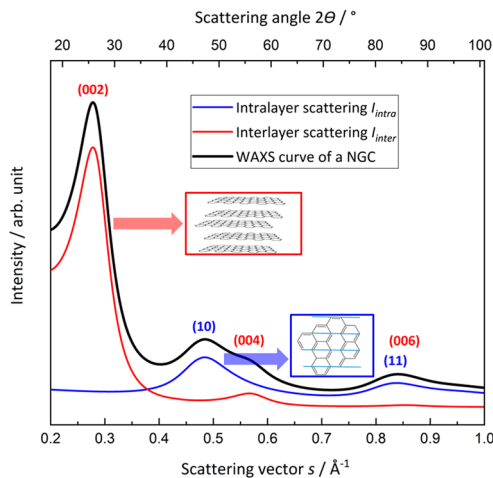


Figure 2. Typical WAXS curve of an NGC resulting from a superposition of intralayer and interlayer scattering intensity. The intralayer scattering generates asymmetric (hk) reflection, the interlayer scattering symmetric $(00l)$ reflections.

further details). As the atomic scattering factor for carbon parallel to the graphene sheets $f_{C,\text{para}}$ is considered to be isotropic, its value equals the tabulated value for the atomic scattering of carbon. With these assumptions, I_{coh} for WAXS is given by

$$\begin{aligned} I_{\text{coh}} = & (1 - c_{\text{un}})(f_{C,\text{perp}}^2 \cdot I_{\text{inter}} + f_{C,\text{para}}^2 \cdot I_{\text{intra}}) \\ & + c_{\text{un}} \cdot f_{C,\text{para}}^2 + c_N \cdot f_N^2 + c_O \cdot f_O^2 \end{aligned} \quad (2)$$

In the aforementioned equation I_{inter} describes the interlayer scattering and depends on the parameters $L_c, \kappa_c, \bar{a}_3, a_{3,\text{min}}, \sigma_3, u_3, \eta, l_{cc}, q$. I_{intra} describes the intralayer scattering and depends on the parameters $L_a, \kappa_a, l_{cc}, \sigma_1, q$. Additional structural parameters, which can be derived by algorithm are $\langle l \rangle$ and $\langle N \rangle$. An explanation of the parameters is given in Figure S1 of the Supporting Information. For further details please refer to our previous publications,^{9,13,14} in particular the original work from 2002.

The incoherent scattering intensity in WAXS arises from Compton scattering by the carbon and is given by its theoretical intensity $I_{\text{com,C}}$. The theoretical values are obtained by interpolation of the values given, for example, in the International Tables for X-ray Crystallography.⁹ As for primary and/or secondary monochromatization specific correction factors have to be taken into account, I_{incoh} is defined as follows, with Q as an optional factor

$$I_{\text{incoh}} = I_{\text{com,C}} \cdot \text{recoil} \cdot Q_{\text{abs}} \cdot Q \quad (3)$$

with recoil as the Breit–Dirac recoil factor, Q_{abs} as the factor for specific absorption of Compton scattering, and Q as an correction term for the attenuation of the Compton scattering due to the finite resolution of a (optional) secondary monochromator. For a definition of these factors, please refer to the Supporting Information of ref 14.

Additionally, for a correct description of the theoretical scattering intensity, the polarization and absorption have to be considered by the polarization factor P and the absorption factor A , respectively. Furthermore, correction of the background by the normalization constant k , the optional tuning of the overall slope of the scattering curve by the factor gFact, and the consideration of a possibly used automatic collimator by

the factor AutoColl are required for a correct description of the theoretical scattering intensity. For these reasons, the theoretical scattering intensity $I_{\text{theoretical}}$ for WAXS is defined as

$$I_{\text{theoretical}} = (1/\text{AutoColl}) \cdot \text{gFact} \cdot k \cdot A \cdot P \cdot (I_{\text{coh}} + I_{\text{incoh}} \cdot Q) \quad (4)$$

with the factors $1/\text{AutoColl}$, gFact, A and Q being optional.

Finally, the intensity of the theoretical scattering curve I_{obs} , which is compared to the logarithmic intensity of the experimentally acquired scattering curves is calculated as

$$I_{\text{obs}} = \log_{10}(I_{\text{theoretical}} + \text{const}_1) + \text{const}_2 \quad (5)$$

The logarithmic representation is used as it eases the comparison of data and fit by the eye. The parameter const_1 and the optional factor gFact are used as in many cases a nonconstant background is observed, which cannot be considered by merely shifting the fit curve vertically (here realized with const_2). Thus, const_1 and gFact were established empirically and have proven themselves useful since then. Please note that the factors AutoColl, A and Q also affect the background and thus should be chosen accordingly before using const_1 and const_2 to consider a background.

The aforementioned algorithm was modified for WANS as described below.

First, the incoherent scattering was disregarded as with neutrons no Compton scattering occurs and the incoherent neutron scattering length of carbon with natural isotopic composition is almost zero (0.001 fm).²² Second, the atomic form factors were replaced by the numerical values of the constant coherent neutron scattering lengths b_{coh} of the respective elements with natural isotopic composition. The values are 6.6460 fm for carbon, 5.803 fm for oxygen, and 9.36 fm for nitrogen. All values were taken from ref 22. Third, the polarization and absorption factors were neglected as carbon does not polarize neutrons and neutron absorption by carbon is insignificant. Fourth, the consideration of a possibly used automatic collimator by the factor was removed as neutron diffractometers usually utilize a Debye–Scherrer geometry. With these modifications the theoretically observable intensity is only proportional to the coherent scattering intensity I_{coh}

$$I_{\text{theoretical}} \propto I_{\text{coh}} \quad (6)$$

For WAXS and WANS, the coherent scattering intensity emerges from the interlayer and intralayer scattering, the scattering from unorganized nitrogen c_N and oxygen c_O impurities, as well as scattering from unorganized carbon c_{un} .¹⁴ In contrast to WAXS the coherent neutron scattering lengths are constant, that is, not a function of the scattering angle θ . Hence, I_{coh} is given by

$$\begin{aligned} I_{\text{coh}} = & (1 - c_{\text{un}}) b_{\text{coh,C}} (I_{\text{inter}} + I_{\text{intra}}) + c_{\text{un}} \cdot b_{\text{coh,C}} + c_N \cdot b_{\text{coh,N}} \\ & + c_O \cdot b_{\text{coh,O}} \end{aligned} \quad (7)$$

Additionally, the correction of the background by the normalization constant k and the optional tuning of the overall slope of the scattering/fit curve by the factor gFact are required for a correct description of the theoretical scattering intensity. Thus, for WANS the theoretical scattering intensity $I_{\text{theoretical}}$ is defined as

$$I_{\text{theoretical}} = \text{gFact} \cdot k \cdot I_{\text{coh}} \quad (8)$$

Finally the intensity of the theoretical scattering curve I_{obs} which is compared to the logarithmic intensity of the

experimentally acquired scattering curves is calculated in the same way as for WAXS. Please note that irregular background patterns caused by the WANS instrument itself must be subtracted from the data before fitting as the data correction terms defined in ref 14 are defined only for WAXS data.

For the samples AC-2400, LSPP-2500, LSPP-2800, and LSPP-3000 Ruland and Smarsly's method could not be applied because of a high degree of graphitization giving rise to (hkl) reflections. As these reflections are not included in the model, fitting the WAXS/WANS patterns of these samples was not possible. Instead, the L_c values were estimated using the Scherrer equation. To determine the FWHM, the 002 reflections were fitted using a Gaussian profile. L_c was subsequently calculated by

$$L_c = \frac{0.093}{\text{FWHM}} \frac{\lambda}{\cos(\theta_{\text{center}})} \quad (9)$$

where θ_{center} is the position of the peak center in the radians.

Experimental Methods. Four different carbon precursors, two graphitizing pitches yielding pitch coke and two non-graphitizing resins yielding glassy carbon, were heat-treated at different temperatures in an inert gas atmosphere using sophisticated temperature programs. In Table 1, the precursor and the maximum treatment temperature of each sample are given. Each sample was kept at the given temperature for 2 h.

Table 1. Overview of the Samples Investigated

sample (abbrev.)	precursor	treatment temp./°C
CB-800	carbon black	800
AC-2400	acetylene coke	2400
PF-N-800	novolac (phenol formaldehyde) resin	800
PF-N-1800	novolac (phenol formaldehyde) resin	1800
PF-R-2100	resole (phenol formaldehyde) resin	2100
PF-R-2800	resole (phenol formaldehyde) resin	2800
MP-1200	mesophase pitch	1200
MP-1800	mesophase pitch	1800
MP-2100	mesophase pitch	2100
LSPP-800	low softening point pitch	800
LSPP-1200	low softening point pitch	1200
LSPP-1800	low softening point pitch	1800
LSPP-2500	low softening point pitch	2500
LSPP-2800	low softening point pitch	2800
LSPP-3000	low softening point pitch	3000

WAXS measurements were performed with a PANalytical XPert Pro powder diffractometer using Cu-K α radiation with an averaged wavelength of $\lambda = 1.5418$ Å. The X-ray tube was operated at 40 kV and 40 mA. A standard Bragg–Brentano θ – θ geometry was used. The powder samples were flattened to a thickness of 1 mm and placed on a silicon single-crystal sample holder. All WAXS measurements were carried out at ambient conditions, that is, ambient pressure and temperature. For all measurements, an automatic divergence slit was used, resulting in an irradiated length of 7 mm on the sample surface. The measurement range for each sample was $10^\circ < 2\theta < 150^\circ$, the step size 0.117° , and scan speed $0.05^\circ/\text{s}$. No background was subtracted from the WAXS data.

WANS measurements were carried out at the flat-cone diffractometer E2²³ and the fine resolution powder diffractometer E9²⁴ at the BER II reactor of Helmholtz-Zentrum Berlin. Both instruments utilize a Debye–Scherrer geometry.

At E2 and E9 the neutron wavelengths $\lambda = 0.92$ and $1.3084(2)$ Å were used, respectively. All powder samples were filled in 6 mm vanadium containers. All WANS measurements were carried out at ambient conditions, that is, room pressure and temperature. At E9, a measurement range of $3^\circ < 2\theta < 142^\circ$ was available, at E2 a measurement range of $4.3^\circ < 2\theta < 102.3^\circ$. The measurement time was 8 h in each case, except for the sample heat treated at 1200 °C for which the measurements lasted for 12 h. For both instruments, the background was recorded by using an empty sample container. The background was subtracted from the WANS data.

The WAXS patterns used to determine the PDFs were acquired at ambient conditions using synchrotron radiation at the Diamond Synchrotron (United Kingdom) beamline I-15-1 (XPDF). The X-rays were monochromatized using a bent Laue monochromator, yielding a wavelength of 0.1734 Å and detected by a PerkinElmer 1621 EN area detector. As sample containers, borosilicate glass capillaries (1 mm in diameter) from Hilgenberg, being spun during data acquisition, were used. Calibration was carried out with a cerium oxide standard and background correction by measuring empty capillaries. DAWN software^{25,26} was utilized for raw data reduction; the PDF were derived by PDFgetX3²⁷ and fitted (see the Supporting Information) by PDFgui²⁸ version 1.1.1. The cut-off used for the Fourier transformation to obtain the PDF was $q_{\text{max}} = 20$ Å⁻¹. The $G(r)$ functions were fitted with one structural phase (graphite, $P6_3mc$) following the procedure outline in the study of Poulain.²⁹ The fit range (r_{max}) was stepwise expanded (2, 20, 60, 80 Å). Finally, a range of 20 Å and 80 Å was used. The following parameters were taken into account: scale factors, linear atomic correlation factor accounting for the effects of correlated motion on the PDF,³⁰ sp diameter (spherical nanoparticle diameter) representing the diameter of the nanoparticle for the PDF shape damping function,³⁰ lattice constants ($a = b, c$), and thermal motion (Debye–Waller-factors $u_{11} = u_{22}, u_{33}$).

Data simulation was carried out by choosing a set of parameters and generating a simulated scattering curve, both for WAXS and WANS. Different levels of Gaussian noise were added to the data and it was truncated at different s -values. This procedure yielded 24 scattering curves for each WAXS and WANS with four different levels of Gaussian noise (0; 0.017; 0.033; 0.5) and six different cut-offs (0.8; 1.2; 1.8; 2.4; 3.0; 3.6) Å⁻¹. Gaussian noise was realized by adding a random number to each point of the simulated scattering curve. The random number was generated using a Gaussian normal distribution with a Mersenne Twister pseudo-random generator. The mean value of the normal distribution μ was set to the y -value of the corresponding point. The noise-level was used as the standard deviation σ of the normal distribution. After generation, the scattering curves were fitted yielding 24 parameter sets each for WAXS/WANS with distinct noise levels and cut-offs. For each parameter of each parameter set the deviation between it and the respective parameter used for simulating the curve was calculated by

$$\text{Deviation}/\% = \frac{\text{parameter}_{\text{original}} - \text{parameter}_{\text{fit}}}{\text{parameter}_{\text{original}}} \times 100 \quad (10)$$

RESULTS AND DISCUSSION

WANS and WAXS Data. Figures 3 and 4 depict the laboratory and synchrotron WAXS data along with the

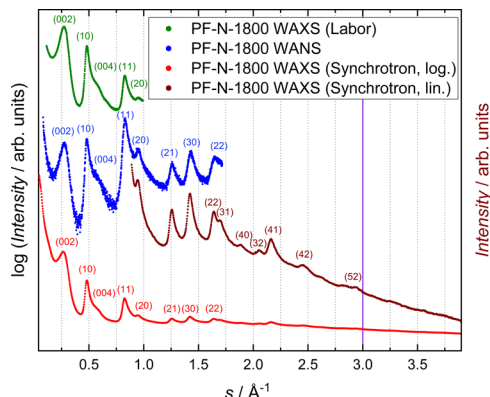


Figure 3. Laboratory and synchrotron WAXS data along with the corresponding WANS data of a novolac resin carbonized at 1800 °C. In all three types of data the typical (hk) and $(00l)$ reflections are present at the same positions (as far as applicable). The purple line at 3 \AA^{-1} indicates the cut-off for the PDF analysis.

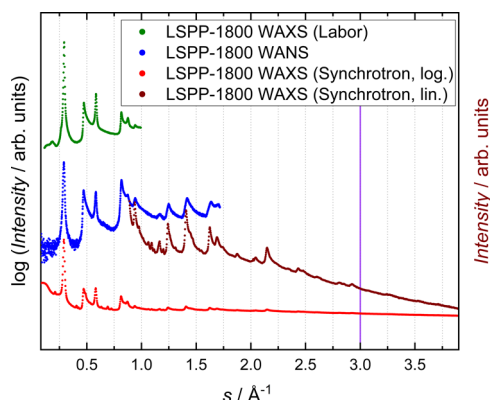


Figure 4. Laboratory and synchrotron WAXS data along with the corresponding WANS data of a low softening point pitch carbonized at 1800 °C. In all data, the typical (hk) and $(00l)$ reflections are present at the same positions (as far as applicable). A high degree of order at the atomic scale is implied by WANS reflections at large s -values, in particular when compared to the WAXS data showing pronounced damping at larger s -values.

corresponding WANS data of a novolac resin and a low softening point pitch, respectively, carbonized at 1800 °C. Please note that the synchrotron data are depicted twice, both logarithmically and linearly scaled. The purple line at $s = 3 \text{ \AA}^{-1}$ indicates the cut-off for the PDF analysis described below. All curves display the typical (hk) and $(00l)$ reflections at the same positions (as far as applicable), indicating a qualitative agreement between the data obtained by the three different measurement methods. In addition, the relative intensities of the reflections are in fair agreement at lower s -values. At higher s -values, the intensity of the synchrotron WAXS reflections is diminished by the atomic form factor, clearly visible by comparison of the logarithmically scaled WANS and WAXS data at s -values larger than 1.25 \AA^{-1} . Thus, although the s -range of the WANS data is limited, its quality is, in comparison to the WAXS data, more suitable for quantitative evaluation, as the WANS reflections are better distinguishable at large s -values.

The presence of reflections at s -values larger than 2.5 \AA^{-1} , here the (42) and (52) reflections, indicates a high degree of order at the atomic scale. A qualitative comparison of both samples (i.e., pitch-based carbon vs resin-based carbon) indicates a more ordered graphene structure for the carbonized low softening point pitch (LSPP-N-1800), as the reflections are more pronounced.

An overview of all the acquired wide-angle scattering curves is provided in the Supporting Information file, see Figures S2–S4.

WAXS/WANS Comparison. Figures 5 and 6 depict the fit of the WANS data of a novolac resin and a low softening point

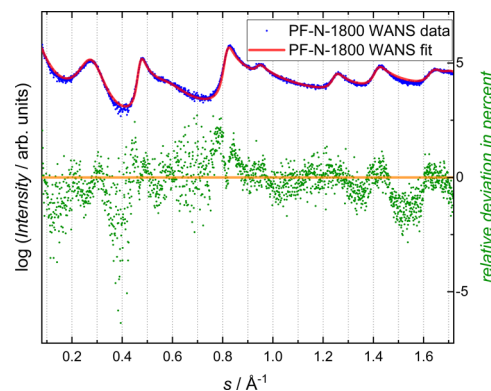


Figure 5. Fit (red solid line) of the WANS data (blue dots) of a novolac resin carbonized at 1800 °C along with relative deviation between fit and data.

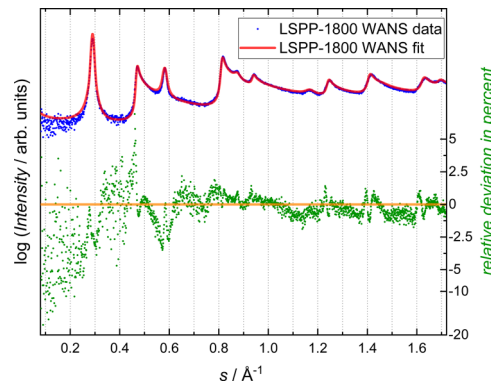


Figure 6. Fit (red solid line) of the WANS data (blue dots) of a low softening point pitch carbonized at 1800 °C along with relative deviation between fit and data.

pitch, respectively, carbonized at 1800 °C. In addition, the relative deviation between fit and data as calculated is shown, defined as

$$I_{\text{dev}} = \frac{I_{\text{experimental}} - I_{\text{obs}}}{I_{\text{obs}}} \quad (11)$$

As there is no significant deviation between data and fit, the fits were judged to be reasonable as described in ref 13.

In Figures 7–9 and Table S1 the parameters obtained from fitting the WANS and WAXS data are given. The average lateral extension L_a and stack height L_c are significantly lower for the samples prepared from a non-graphitizing resin precursor compared to the samples made from graphitizing low softening point pitch precursors, for the same heat-

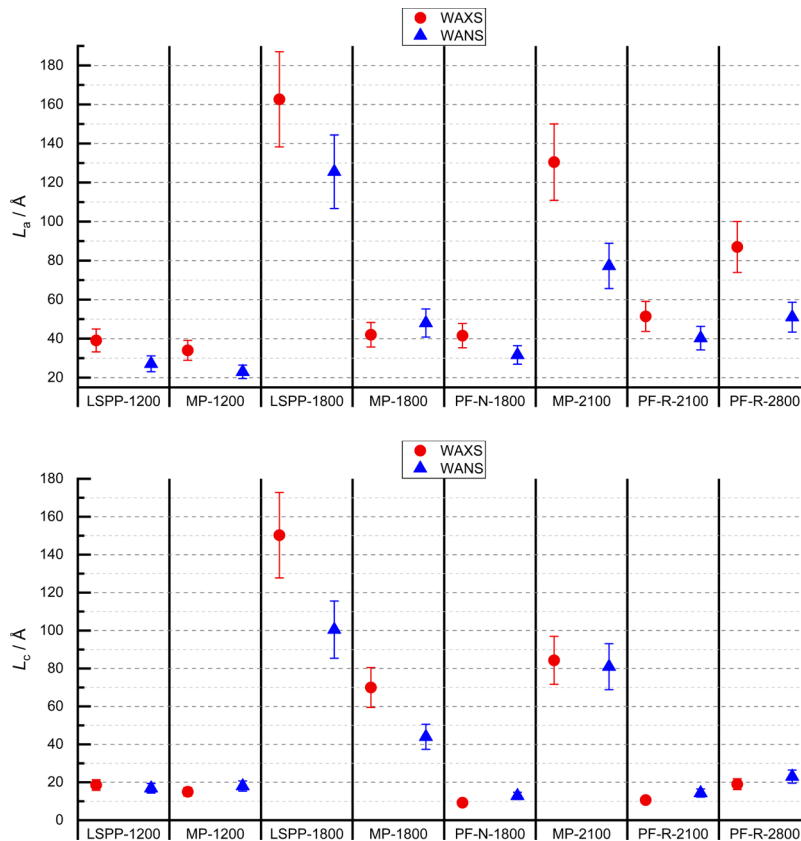


Figure 7. Comparison of the microstructural parameters L_a & L_c for eight samples, graphitizing (LSPP-1200, MP-1200, LSPP-1800, MP-1800, and MP-2100) and non-graphitizing ones (PF-N-1800 and PF-R-2100, PF-R-2800), obtained from WANS and WAXS analyses using the approach of Ruland and Smarsly. These size parameters mostly match within the respective error margins or possess at least the same order of magnitude.

treatment temperature. This finding is in accordance with literature. Even if carbonized at 2800 °C, the PF-R-2800 sample only yields L_a and L_c values smaller than those of the LSPP-1800 sample carbonized at 1800 °C. In contrast, at 1800 °C, the average lateral extension L_a of the PF-N-1800 sample is comparable to the average lateral extension of the MP-1800 sample. For the LSPP samples, a significant increase in L_c and L_a is observed with increasing carbonization temperature. These values of the LSPP-1800 sample surpass those of the MP-2100 sample, and this difference is in accordance with reports found in literature.^{5,31} In general, for the samples made from mesophase pitch (MP-1200, MP-1800), the increase in L_c and L_a with increasing carbonization temperature is less pronounced. Comparing the structural parameters determined from WAXS and WANS, the L_a and L_c values match within their respective error margins or possess at least the same order of magnitude, with few exceptions. However, for most of the samples the absolute values of L_c and L_a are similar. Also, the trends in these two parameters for the LSPP and MP samples, as a function of treatment temperature, are identical for the WAXS and WANS analyses, that is, L_a and L_c grow significantly at 1800 °C compared to 1200 °C. The parameters derived from WANS are considered to be more trustworthy because of a larger underlying s -range and enhanced WANS data quality compared to WAXS.

The C–C bond length l_{CC} is comparable for all samples and lies in the range typically observed for NGCs. The average distance between the layers \bar{a}_3 lies above that of graphite, being lower for the samples prepared from a graphitizing precursor in comparison to the resin-based samples carbonized at 1800 °C

and 2100 °C, respectively, which underpins the fundamental differences between such carbon precursors. Hence, for the PF-R-2800 sample the value is comparable to \bar{a}_3 of pitch-based samples carbonized at lower temperatures. For the LSPP samples, a decrease in \bar{a}_3 with increasing heat treatment temperature is observed. The l_{CC} and \bar{a}_3 parameters all match within their respective error margins indicating good agreement between WAXS and WANS data. It should be noted that the deviations neglecting the error range are more pronounced for the PF-N-1800, PF-R-2100, and PF-R-2800 samples, all made from a non-graphitizing precursor.

The parameters quantifying the degree of disorder in the stacking (σ_3) and the layers themselves (σ_1) are of particular interest with respect to the question, if WANS data provide more reasonable and meaningful values. We find σ_3 and σ_1 derived from WANS data to be larger for the PF-N-1800 and PF-R-2100 samples (resin-based carbons) compared to the LSPP and MP samples, for the same or even larger carbonization temperature. This trend has been previously described in ref 31. For the PF-R-2800 sample, these values are solely lower than those of the pitch-based samples carbonized at 1200 °C. For σ_3 derived from the WAXS data the value of the PF-N-1800 sample is nearly the same as for the MP-1200 and MP-1800 samples, all exceeding these values of the LSPP samples. For the PF-R-2100 and PF-R-2800 samples σ_3 is lower than the MP-1200 and MP-1800 sample but exceeds σ_3 of the MP-2100 sample. For σ_1 derived from WAXS data, no clear tendency is visible. In addition, the σ_1 -values obtained from WAXS and WANS data differ significantly. As the WANS data display a larger number of reflections because of their

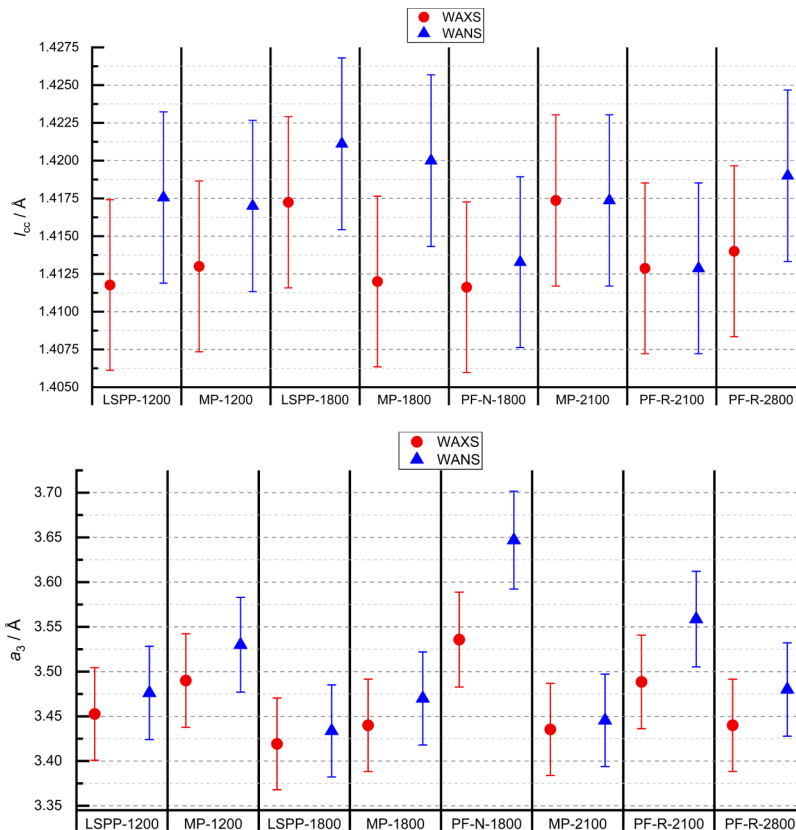


Figure 8. Comparison of the microstructural parameters l_{cc} & \bar{a}_3 for eight samples, graphitizing (LSPP-1200, MP-1200, LSPP-1800, MP-1800, and MP-2100) and non-graphitizing ones (PF-N-1800 and PF-R-2100, PF-R-2800), obtained from WANS and WAXS analyses using the approach of Ruland and Smarsly. These size parameters mostly match within the respective error margins.

larger s -range allowing for a clearer separation of size and disorder effects and possess an enhanced data quality in terms of physical limitations, the values derived from WANS data should be considered more trustworthy. This conclusion is supported by the more pronounced difference between the disorder parameters retrieved from WANS data of the samples made from graphitizing and non-graphitizing precursors, such trend being described in literature previously.

The WAXS and WANS data acquired for the samples exposed to higher temperatures (2500, 2800, and 3000 °C) exhibit reflections of graphitic carbon, which prevents the application of the analytical approach of Ruland/Smarsly. Hence, these WAXS and WANS data were not analyzed in further detail. However, in order to reveal qualitative trends upon treatment at such high temperatures, the (002) reflection of the WAXS and WANS data were analyzed using the Scherrer analysis. The results are given in the Supporting Information file (Table S2 and Figure S5). The values of the domain size obtained from the WAXS data show a clear trend—the stack height grows with increasing carbonization temperature, which is in accordance with literature.³¹ From the WANS data, in contrast, for all carbonization temperatures, roughly the same stack height is retrieved, that is, a substantial deviation between WAXS and WANS with increasing carbonization temperature is found. This effect is caused by the larger instrumental broadening for WANS compared to the WAXS, which obscures the true FWHM of the reflections caused by the sample only. This effect does not impair the analysis using Ruland's and Smarsly's algorithm as this algorithm is only applicable for samples carbonized at temperatures far below

2400 ° (if made from a graphitizing precursor). At this temperature, the L_c values retrieved from both WANS/WAXS match within the respective error margins. For samples made from a non-graphitizing precursor the instrumental broadening of the WANS instruments has no effect, too, because of the relatively low stack height (23 Å) found even at carbonization temperatures of 2800 °C. Even at such high temperatures, the signals are quite broad, being larger than the instrumental broadening.

Simulated Data. As for most of the parameters relatively large error bars were found, the question arises, if the used evaluation approach is in principle capable of providing accurate and precise structural parameters from WANS or WAXS data at all. Hence, in this subsection we generated simulated WANS and WAXS data of NGCs to estimate the minimal data quality required for a precise and accurate fit and also to assess the range of uncertainty in the determination of these structural parameters from experimental WANS as well as WAXS data. Two modifications were applied to the simulated WANS and WAXS patterns in order to mimic realistic experimental conditions: first, the simulated WANS/WAXS data were cut at certain s -values to thereby simulate a limited or an extended s -range. Second, the WANS/WAXS data were blurred applying different levels of statistical noise (see the Experimental Section for details). These simulated “experimental” WAXS/WANS data, depicted in Figure 10, were then analyzed using Ruland and Smarsly's approach. These analyses provided a set of structural parameters as described above for each combination of cut-off and noise-level. In order to elucidate the impact of these two factors on

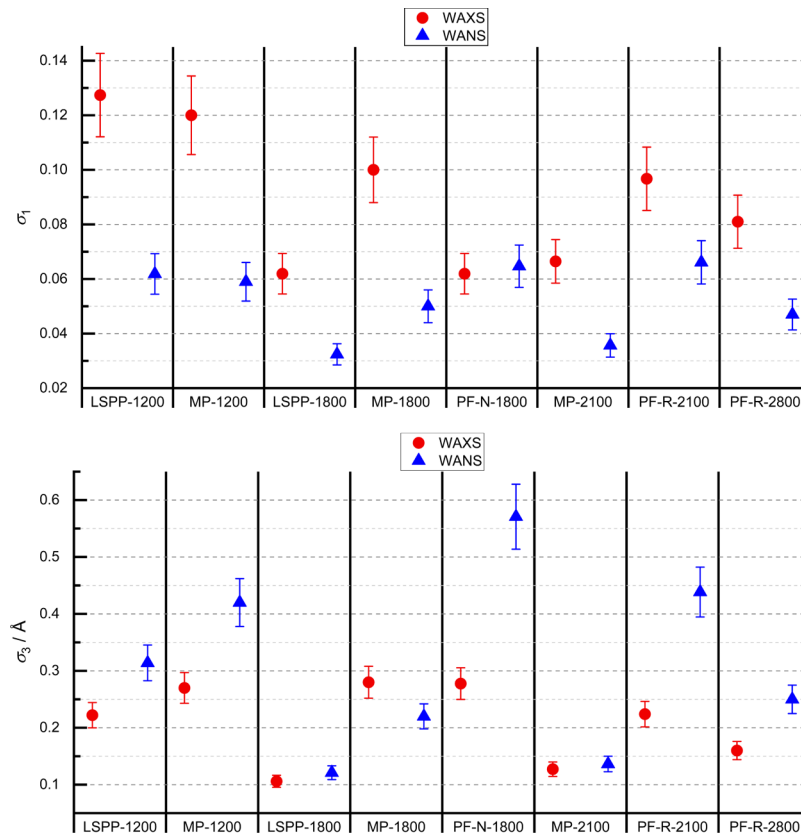


Figure 9. Comparison of microstructural parameters σ_1 & σ_3 for eight samples, graphitizing (LSPP-1200, MP-1200, LSPP-1800, MP-1800, and MP-2100) and non-graphitizing ones (PF-N-1800 and PF-R-2100, PF-R-2800), obtained from WANS and WAXS analyses using the approach of Ruland and Smarsly. The deviations of these disorder parameters between the WAXS and WANS analyses are supposedly caused by the higher number of reflections available in our WANS data and thus a better distinction between size and disorder effects.

the accuracy and precision of the evaluation, these parameters were then compared with the original parameter values. By this procedure, it was possible to assess which of the two factors (limit s -range and noise) dominates the accuracy/uncertainty in the parameter determination.

The parameters yielded from fitting the impaired simulated data are given in **Tables S3 and S4** along with the parameters used for simulation. A graphical overview of the deviations from the respective original values is given in **Figures 11** and **12**. For WANS, the interlayer parameters are mostly unaffected by lower cut-offs but strongly affected by noise (see the Experimental Section for the definition of the noise). Whereas from noise-free scattering curves the parameters used for simulation were in exact agreement with the original ones, increasing the noise-levels leads to significant deviations. For L_c , the deviation increases from 0% at a noise-level of 0 to 7.7% at a noise level of 0.05 (as defined above). \bar{a}_3 and σ_3 show, in principle, the same trend with a few aberrations. It should be noted that \bar{a}_3 can be reconstructed much more precisely and accurately than L_c and σ_3 , having a maximal deviation of merely 0.6%.

The intralayer parameters are affected by both noise and cut-off. Interestingly, a higher cut-off (i.e., a larger accessible s -range) leads to larger deviation of L_a as the deviation increases from 0% up to 10.3% for the largest noise-level and cut-off. A similar trend can be observed for l_{CC} . For this parameter, the deviation is in comparison small and considered to be negligible. For σ_1 , a reverse trend becomes apparent—the deviation increases in general with increasing noise but

decreases in general with larger cut-off values. The maximum deviation for this parameter—20%—is about twice the maximum deviation of L_a .

The reason for the different trends in the reconstruction of inter- and intralayer parameters from simulated WANS data lies to a large extent with the diminishing intensity of the reflections at large s -values. The interlayer parameters are derived from a relatively small number of reflections (only (001) reflections), whereas for the intralayer parameters a large number of reflections (hk) is present. In general, disorder effects result in a widening of reflections with increasing s , whereas a limited size L_a leads to a constant width of the reflections of one particular lattice plane family; that is, the (002) reflection has the same width as the (004) reflection, if disorder (stress/strain) is absent and if the width is thus only determined by the finite dimension in this crystallographic direction. On the basis of these considerations, the disorder parameter σ_1 is determined more accurately using a larger s -range, as the impact of a larger number of reflections entering the analysis overcomes the influence of more noisy data points. In other words, the impact of disorder on the signal widths can be separated more reasonably, as the quantification of the increasing width requires a sufficient number of reflections.

In contrast to σ_1 the uncertainty in determining the original value of L_a rises with an increased accessible s -range, which might be regarded as counterintuitive. The decrease in σ_1 necessarily needs to be associated with a decrease in L_a to maintain the same overall width of the single (hk) reflections, if different cut-off limits are compared. Hence, we assume that

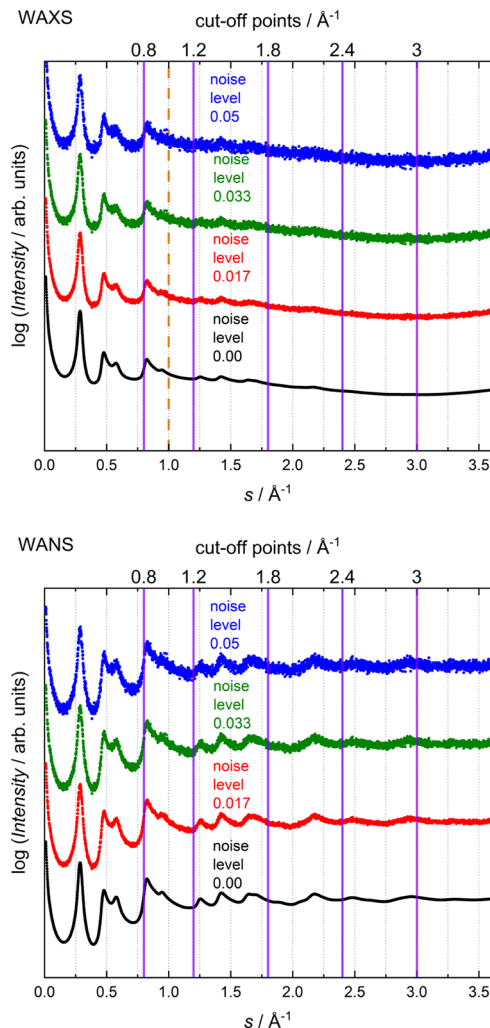


Figure 10. Overview of the simulated “experimental” WAXS/WANS data. The noise level decreases from top to bottom. The vertical purple lines indicate the cut-off points, the dotted orange line the typical s -range of a laboratory setup X-ray diffractometer using $\text{Cu}-\text{K}\alpha$ -radiation. A distinct difference between WANS and WAXS is visible, that is, a significant dampening of the latter at large s -values.

for such types of data the impact of σ_1 is more decisive in obtaining a reasonable fit over the entire s -range, which in turn governs the trend in L_a .

For WAXS, similar trends can be observed for the interlayer parameters. For L_c and \bar{a}_3 the maximum deviation for WAXS (18.0% for 0.05 noise and a 0.8 \AA cut-off) is larger than for WANS. The deviations for σ_3 lie in the same range. Regarding the intralayer parameters again a negligible deviation for l_{CC} is found. For L_a a maximum deviation of 24.1% is found for WAXS—more than double the value of the maximum L_a deviation for WANS (10.3%). Interestingly, for σ_3 the maximum deviation for WAXS (12.0%) is lower than for WANS (20.0%).

In conclusion, these analyses of simulated, blurred WANS/WAXS data allow for a qualitative assessment of the influence of limited s -range and noise on the determination of important and meaningful structural parameters. We find that data noise generally exerts a larger negative impact on the WAXS/WANS analysis than a limited s -range, whereas the precision in the parameter values is higher for WANS compared to WAXS. Unfortunately, especially the most relevant parameters L_a , L_c ,

σ_1 , and σ_3 are associated with a significant error in the range of ca. 10% in the case of medium data noise. However, such precision is sufficient for semiquantitative comparisons among similarly treated materials, for example, as a function of temperature. Hence, as a main finding even standard laboratory WAXS instruments, using the averaged $\text{Cu}-\text{K}\alpha$ wavelength of 1.5418 \AA , will provide a sufficient data quality for determining these parameters with the precision needed for a meaningful interpretation.

PDF Analysis. Figure 13 summarizes the PDF analysis of the different NGC samples. Additionally, the PDF of a carbon with a quite ordered microstructure (AC-2400, derived from acetylene coke) was determined, serving as reference for the “disordered” pitch- and resin-based carbons under study, in particular with respect to the width of the maxima and the damping toward large r -values. The acetylene coke sample exhibits a large degree of order as evidenced by distinct WANS reflections (see the Supporting Information file), because of the high carbonization temperature ($2400 \text{ }^\circ\text{C}$), which is expected for such type of carbon. Consequently, the maxima in the PDF are well defined, possess a comparably small width, and the entire curve shows only moderate damping, in comparison to the other samples under study. For small interatomic distances, that is, the first few atomic neighbors, the maxima match those of graphite quite well for all materials. Interestingly, the PDF curves of all samples exhibit a relatively small width of the maxima at small distances, matching the shape of the PDF of acetylene coke below 6 \AA , even for the non-graphitizing samples (PF-N-1800). At larger distances, all of the PDFs of the NGC under study damp significantly, which is in agreement with the substantial disorder as quantified by the WAXS/WANS fitting approach. The high degree of order within the first few benzene rings, found for all the samples, is in excellent agreement with the appearance of distinct high-order reflections at large s -values in the WAXS synchrotron and also WANS data (see the section **WANS and WAXS Data**). Note that no atomic distances corresponding to the layer distance are observed in the PDFs because of the turbostratic nature of the graphene stacking.

As maxima in PDF curves can be substantially influenced and generated by cut-off and other numerical affects, the PDF of graphene was simulated by utilizing the crystallographic information file (CIF) file of graphite, the same cut-off as in the experimental data ($q_{\max} = 20 \text{ \AA}^{-1}$), and enhancing the layer distance to 60 \AA (see the Supporting Information, Figure S6). The comparison of such simulated PDF with experimental data (here for two samples, AC-2400 and PF-N-1800 representing a more disordered carbon) reveals certain maxima to be ripples because of numerical effects, but most of the pronounced maxima are indeed attributable to the graphene lattice. This analysis justifies the validity of the determination of the PDF itself at distances below distances of ca. 15 \AA and the qualitative interpretation derived therefrom. However, at larger distances the deviation between the PDF and the theoretical graphene structure becomes significant (see discussion below).

Hence, the PDF determined for the samples under study allows for a meaningful qualitative comparison in terms of the graphene dimension and disorder. The degree of order grows with increasing heat treatment temperature, as seen by a narrowing of the signals, being more pronounced for the pitch-based sample than for the resin-based sample. Although in general the width of the maxima of the $G(r)$ function in real space is affected by the Debye–Waller factor, such qualitative

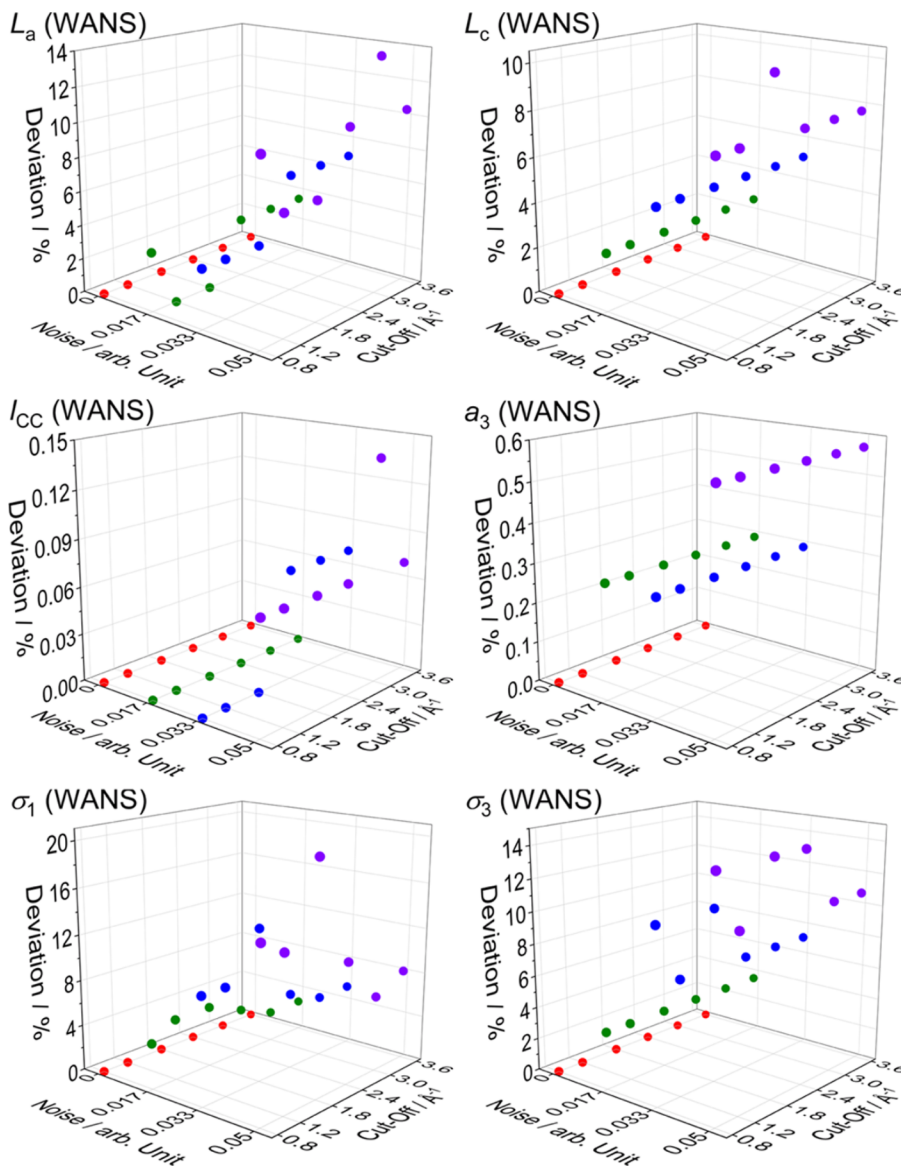


Figure 11. Overview of the relative deviation between the parameters used for data simulation and the parameters obtained by fitting the impaired data for WANS. Impairing was carried out by both truncating the data at different s -values and adding different levels of Gaussian noise. The deviation was calculated by dividing the absolute value of the differences between the parameters used for simulation and the parameters obtained from fitting by the parameters used for simulation. Dots of the same color share the same cut-off; the noise-level increases from red via green and blue to purple dots.

interpretation is legitimate, as all samples were measured at the same temperature. The resin-based sample carbonized at 1800 °C exhibits at interatomic distances larger than 6 Å a lower degree of order than the pitch-based sample carbonized at the same temperature, which is supported by the trend in the σ_1 -values found in the previous sections. For all samples, the PDFs thus show two distinct regions, that is, pronounced and sharp signals at distances below ca. 6 Å and smeared/broad maxima at larger distances, and for the distances below ca. 6 Å the PDFs are quite similar for quite different carbons.

The PDFs of the pitch-based samples treated at 800, 1200, and 1800 °C agree with the PDF of acetylene coke up to ca. 8 Å, beyond which the PDFs are damped significantly. Surprisingly, the PDFs of the resin-based carbons are quite similar to that of AC-2400 up to 6 Å, which is thus only slightly smaller than in the case of the pitch-based samples. This finding is remarkable, as the disorder parameter σ_1 obtained

from the fitting approach is substantially smaller for the pitch-based carbons in comparison with resin-based carbons, and also the L_a values are substantially larger for the pitch samples in comparison with the resin-based samples. Hence, the PDF analysis, the L_a and the σ_1 values altogether suggest that there are two different structural graphene-related features which need to be considered in interpreting the evolution of size and disorder upon heat treatment, namely, on the sub-nanometer level and on the level of >5 nm.

In general, the damping of the PDF can be correlated to an average particle size, in this case the graphene extent, and to disorder effects. Although the L_a values do not directly relate to an average diameter of coherent graphene areas, one can calculate a corresponding diameter assuming a circular shape of the graphenes by $L_a = 16R/3\pi$, as shown in 2002.⁹ Using this relationship provides values for the radius, being convertible in a diameter D which is similar to L_a itself ($L_a =$

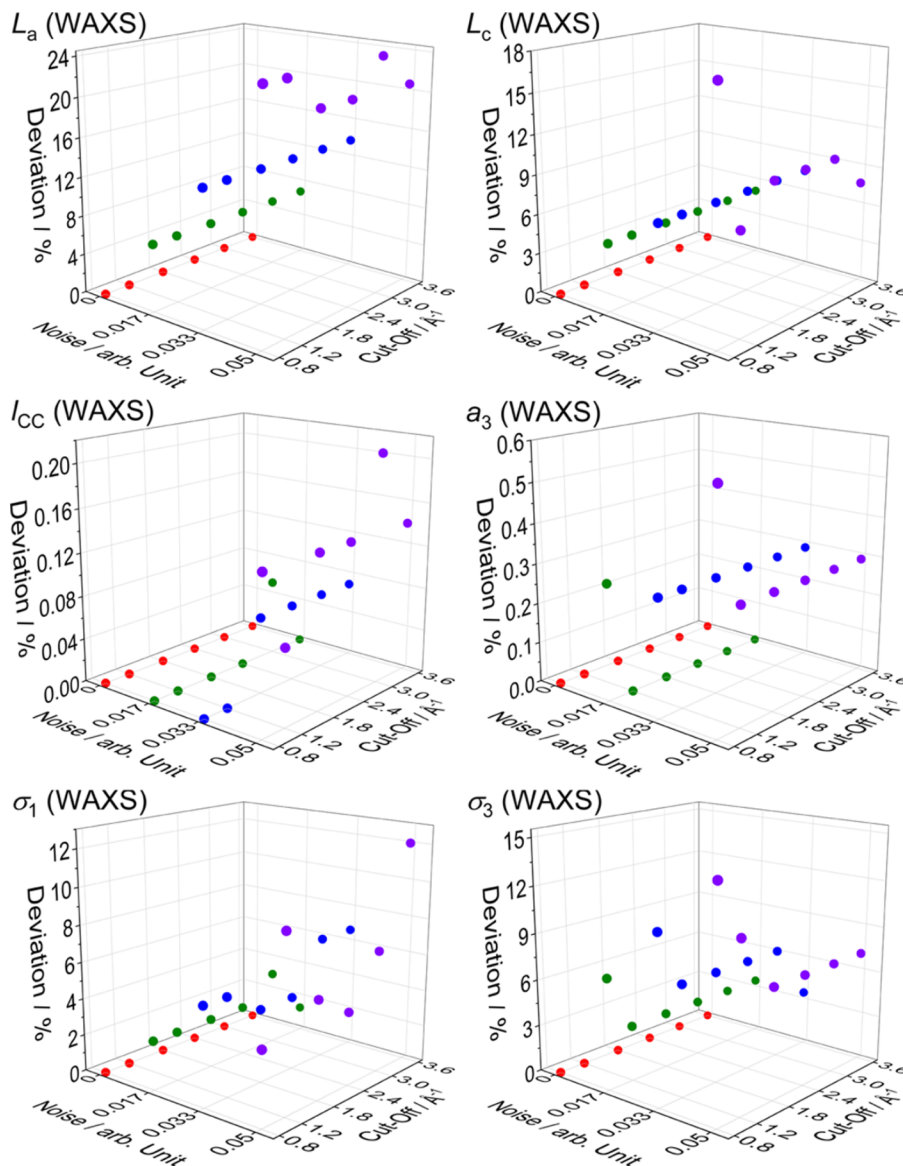


Figure 12. Overview of the relative deviation between the parameters used for data simulation and the parameters obtained by fitting the impaired data for WAXS. Impairing was carried out by both truncating the data at different s -values and adding different levels of Gaussian noise. The deviation was calculated by dividing the absolute value of the differences between the parameters used for simulation and the parameters obtained from fitting by the parameters used for the simulation. Dots of the same color share the same cut-off; the noise-level increases from red via green and blue to purple dots.

0.85 D). Interestingly, for all samples except AC-2400 the L_a values and thus the graphene diameters are substantially larger than the extent of high structural order observed in the PDF (ca. 5–8 Å) as depicted in Figure 14.

It is in principle possible to extract a particle dimension directly from the PDF itself. Using a spherical shape factor to model the effect of finite nanoparticle size allows for retrieving the sp diameter d_{sp} . Using the PDFgui software as described above, first the influence of the parameter u_{33} on the obtained sp diameters was investigated. As depicted in Figures S7 and S8 (see the Supporting Information), the fit quality without and with fixed u_{33} is similar, which is supported by the similar sp diameters obtained from those fits. Therefore, the effect of the u_{33} parameter can be assumed to be negligible. In contrast, fixing the sp diameter to a value of 15 Å, which is below the value obtained from a constraint-free fit, leads to a significantly worse fit indicated by the onset of the dampening at a

significant lower r -value (see Figure S9 in the Supporting Information). Thus, we assume the obtained sp diameters to be at least qualitatively comparable among each other. A complete overview of the fitting results is provided in Table S5 in the Supporting Information.

In Figure 13, an overview of all fits of the PDF is included. To assess the fit quality, data and fit are only shown up to 20 Å. In the case of the carbons with high order (PF-N-1800, LSPP-1200, LSPP-1800, AC-2400) the fits are reasonable only up to ca. 12 Å but at larger distances systematic deviation is observed. For samples of lower order, the fitting is reasonable up to ca. 8 Å only, because substantial damping is observed. For all samples, the sp diameter is smaller than the average lateral extension L_a as also depicted in Figure 14, with the difference being more pronounced for the samples heat-treated at higher temperatures. For both d_{sp} and L_a the same trend, an increase with increasing heat treatment temperature, is found.

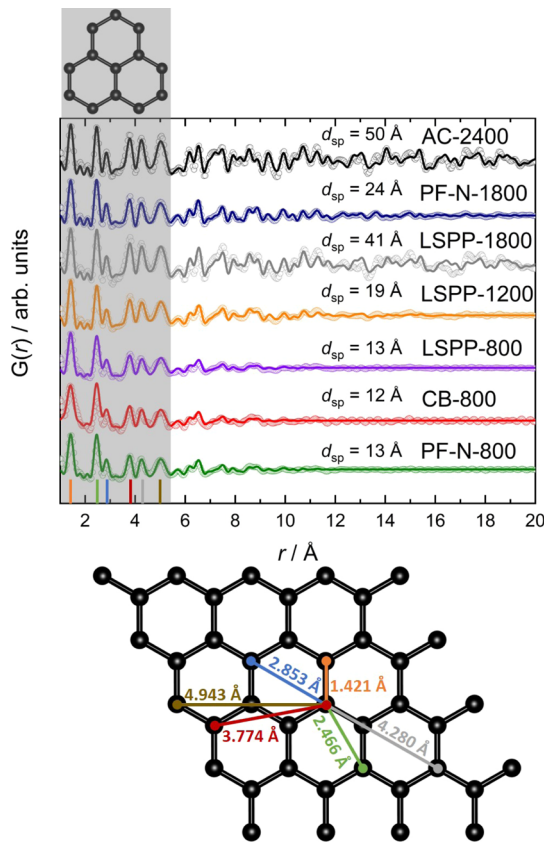


Figure 13. PDF data of different NGC samples and fit of those data without constraints up to 20 Å (80 Å for the AC-2400 and LSPP-1800 samples). For small interatomic distances, the values obtained match those of graphite. Hence, at the atomic level, a high degree of order is found, corresponding to a defined polycyclic structure. The gray zone indicates the maximum distance in phenalene, serving as a comparison. This view is further supported by the relatively small width of the maxima at small distances. Although the width is influenced by the Debye Waller factor, this qualitative interpretation is legitimate, as all samples were measured at the same temperature.

We assume the discrepancy to be caused by different modeling approaches. While Ruland and Smarsly's algorithm considers both, size and disorder, the disorder is neglected in the PDF analysis. Thus, the apparent disorder causes the particle size being calculated to be too small. A complete overview of the fitting results is provided in Table S6 in the [Supporting Information](#).

On the basis of these qualitative findings we conclude that the WAXS/WANS fitting and the PDF analysis speak for a peculiar structure of the graphenes, and we propose a structural model for NGCs as depicted in Figure 15, which goes beyond the previously favored view on the structure of NGCs. In this model, each layer is divided into one or more highly ordered domains ("core(s)") surrounded by a less-ordered region within one graphene. These "core" domains typically extend to several benzene rings as revealed by the PDF analysis. It thus seems that small defined polycyclic aromatic units form already at quite moderate temperatures and do not substantially grow up to temperatures of even up to 2100 °C, which is a surprising result. At first glance, the preservation of such small oligoaromatic units seems to be in contradiction with the pronounced increase in the L_a values. However, L_a represents an average value for the extent of

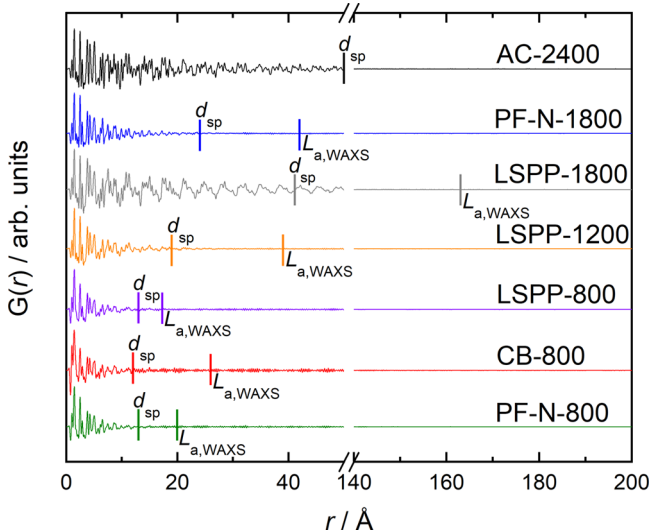


Figure 14. PDF data of all samples shown up to 200 Å with a break from 50 to 140 Å together with the obtained d_{sp} -values (assuming spherical particle shape) and corresponding L_a values. The d_{sp} value obtained is lower than L_a for all samples and the PDF dampens far below the graphene diameters determined by fitting wide-angle scattering (WAXS/WANS) data.

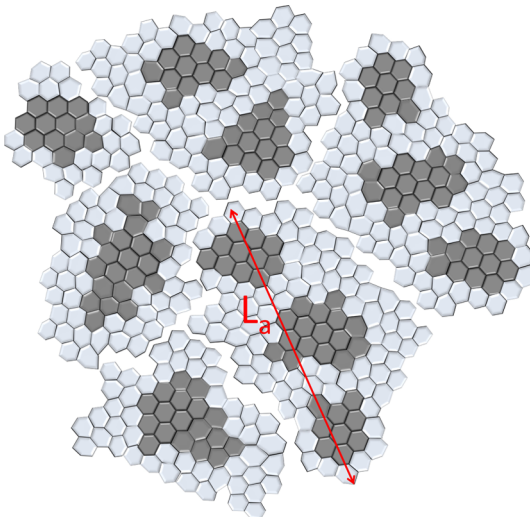


Figure 15. Assumed structures of the graphene layers found in NGCs. Either only one highly ordered core is surrounded by a less-ordered shell or more than one ordered core is present. Please note that the figure is not true to scale.

graphenes, and the underlying WAXS/WANS analysis probes both, highly ordered units as well as sp^2 -regions with less structural order. Hence, approaches such as the evaluation of Ruland and Smarsly are hardly able to resolve such two populations. In contrast, PDF analysis is sensitive to local order on the sub-nanometer scale, and regions with substantial structural disorder would hardly be visible in the PDF graphs next to highly ordered structural units.

One might argue that the small ordered domains should result in a corresponding contribution at large s in WAXS/WANS data, where the (hk) reflections of the less-ordered graphene regions are damped out. However, typically WAXS/WANS data are acquired up to relatively small maximum s values, whereas the scattering data used for PDF

analysis are taken up to quite large s , which corresponds to small structural units. Thus, the contributions of the regions of different order both contribute to WAXS/WANS data, and the applied fitting analysis inevitably results in average structural parameters, whereas the PDF analysis allows for discriminating especially the small-ordered regions.

CONCLUSIONS

In the present study, different types of NGCs were studied by WAXS and WANS, the latter providing scattering data at larger scattering vectors than standard X-ray laboratory instruments. Given the substantial width of the reflections, a major goal was to elucidate the disorder in such carbons based on a thorough analysis of the WAXS/WANS data.

The WAXS/WANS data were analyzed by Ruland and Smarsly's model for NGC microstructural analysis, which is based on fitting the entire WAXS/WANS curve using suitable theoretical model functions. This approach was adopted for WANS, providing an excellent fit to the experimental WANS data. Thus, this model is a comprehensive tool for the microstructural analysis based on any wide-angle scattering technique. WANS, at first glance, seems to be advantageous, as WANS data are not impeded by the non-constant atomic form factor in X-ray scattering and pronounced Compton scattering. The good agreement of size parameters obtained from both WANS and WAXS data analysis, however, proves that despite experimental limitations, including the limited s -range accessible with standard laboratory XRD setups, WAXS analyses yield meaningful values for the microstructural parameters such as L_a and L_c . The disorder parameters, in contrast, profited from the enhanced WANS data quality.

However, fitting procedures do not necessarily provide physically meaningful structural information, as a reasonable fit just corresponds to a mathematical optimization. Hence, further insights into the quality of the used approach were obtained by analysis of blurred simulated WAXS and WANS data, under variation of a statistical noise level and the accessible s -range. It was found that from simulated WANS and WAXS data, endowed with a noise-level being comparable to experimental data, the original parameters were reasonably reconstructed. For medium noise levels, especially the most relevant parameters L_a , L_c , σ_1 , and σ_3 are already associated with a significant error in the range of ca. 10–15%. However, such precision is still sufficient for semiquantitative comparisons among similarly treated materials, for example as a function of temperature. In conclusion, our study proves that standard laboratory WAXS instruments, using the averaged Cu-K α wavelength of 1.5418 Å, are suited for NGC microstructural analysis and provide meaningful values of relevant structural parameters.

The WAXS and WANS analyses were complemented by PDF analyses on the same samples, the comparison showing surprising features and insights into the nanoscaled polycyclic aromatic structure of NGCs. It was found that all NGC's, even samples such as resin-based carbons with quite disordered overall graphene structures, exhibit highly ordered small oligoaromatic units with a size far below L_a surrounded by a less-ordered sp² region. These ordered, small domains grow only moderately up to temperatures of 1800 °C, although the coherent graphene size (determined by WAXS/WANS) is markedly increased, up to dozens of nanometers. We believe that this insight represents an important modification of the general view on the microstructure of carbon materials in

general. However, our study did not clarify the exact spatial size and distribution and relative concentrations of these small, highly ordered domains, that is, the exact size and number of such core(s) per layer. Such details will be subject to further studies particularly encompassing in-depth quantitative PDF analyses.

ASSOCIATED CONTENT

Supporting Information

The Supporting Information is available free of charge on the ACS Publications website at DOI: [10.1021/acs.jpcc.9b03590](https://doi.org/10.1021/acs.jpcc.9b03590).

Parameters used by Ruland and Smarsly's algorithm, acquired wide-angle scattering curves, WAXS/WANS comparison results, Scherrer analysis results, data simulation results, and PDF simulation results ([PDF](#))

AUTHOR INFORMATION

Corresponding Author

*E-mail: bernd.smarsly@phys.chemie.uni-giessen.de.

ORCID

Wolfgang G. Zeier: [0000-0001-7749-5089](#)

Bernd M. Smarsly: [0000-0001-8452-2663](#)

Author Contributions

[†]T.P. and F.M.B. contributed equally to this work.

Notes

The authors declare no competing financial interest.

ACKNOWLEDGMENTS

The authors thank HZB for the allocation of neutron radiation beamtime and thankfully acknowledge the financial support from HZB. This work was supported by Diamond Light Source (beamtime award EE13560) with beamtime proposal SP13560. Financial support is provided by the German Research Foundation (DFG) via the GRK (Research Training Group) 2204 "Substitute Materials for sustainable Energy Technologies".

REFERENCES

- (1) Warren, B. E. X-Ray Diffraction in Random Layer Lattices. *Phys. Rev.* **1941**, *59*, 693–698.
- (2) Fitzer, E.; Kochling, K.-H.; Boehm, H. P.; Marsh, H. Recommended terminology for the description of carbon as a solid (IUPAC Recommendations 1995). *Pure Appl. Chem.* **1995**, *67*, 473–506.
- (3) Adelhelm, P.; Cabrera, K.; Smarsly, B. M. On the use of mesophase pitch for the preparation of hierarchical porous carbon monoliths by nanocasting. *Sci. Technol. Adv. Mater.* **2012**, *13*, 015010.
- (4) Krüner, B.; Schreiber, A.; Tolosa, A.; Quade, A.; Badaczewski, F.; Pfaff, T.; Smarsly, B. M.; Presser, V. Nitrogen-containing novolac-derived carbon beads as electrode material for supercapacitors. *Carbon* **2018**, *132*, 220–231.
- (5) Badaczewski, F.; Loeh, M. O.; Pfaff, T.; Dobrotka, S.; Wallacher, D.; Clemens, D.; Metz, J.; Smarsly, B. M. Peering into the structural evolution of glass-like carbons derived from phenolic resin by combining small-angle neutron scattering with an advanced evaluation method for wide-angle X-ray scattering. *Carbon* **2019**, *141*, 169–181.
- (6) Shi, H.; Reimers, J. N.; Dahn, J. R. Structure-refinement program for disordered carbons. *J. Appl. Crystallogr.* **1993**, *26*, 827–836.
- (7) Azuma, H. New Structural Model for Nongraphitic Carbons. *J. Appl. Crystallogr.* **1998**, *31*, 910–916.
- (8) Fujimoto, H.; Shiraiishi, M. Characterization of unordered carbon using Warren–Bodenstein's equation. *Carbon* **2001**, *39*, 1753–1761.

- (9) Ruland, W.; Smarsly, B. X-ray scattering of non-graphitic carbon: an improved method of evaluation. *J. Appl. Crystallogr.* **2002**, *35*, 624–633.
- (10) Zickler, G. A.; Smarsly, B.; Gierlinger, N.; Peterlik, H.; Paris, O. A reconsideration of the relationship between the crystallite size La of carbons determined by X-ray diffraction and Raman spectroscopy. *Carbon* **2006**, *44*, 3239–3246.
- (11) Hu, Y.-S.; Adelhelm, P.; Smarsly, B. M.; Hore, S.; Antonietti, M.; Maier, J. Synthesis of Hierarchically Porous Carbon Monoliths with Highly Ordered Microstructure and Their Application in Rechargeable Lithium Batteries with High-Rate Capability. *Adv. Funct. Mater.* **2007**, *17*, 1873–1878.
- (12) Faber, K.; Badaczewski, F.; Oschatz, M.; Mondin, G.; Nickel, W.; Kaskel, S.; Smarsly, B. M. In-Depth Investigation of the Carbon Microstructure of Silicon Carbide-Derived Carbons by Wide-Angle X-ray Scattering. *J. Phys. Chem. C* **2014**, *118*, 15705–15715.
- (13) Faber, K.; Badaczewski, F.; Ruland, W.; Smarsly, B. M. Investigation of the Microstructure of Disordered, Non-graphitic Carbons by an Advanced Analysis Method for Wide-Angle X-ray Scattering. *Z. Anorg. Allg. Chem.* **2014**, *640*, 3107–3117.
- (14) Pfaff, T.; Simmernacher, M.; Smarsly, B. M. CarbX: a program for the evaluation of wide-angle X-ray scattering data of non-graphitic carbons. *J. Appl. Crystallogr.* **2018**, *51*, 219–229.
- (15) Puech, P.; Dabrowska, A.; Ratel-Ramond, N.; Vignoles, G. L.; Monthoux, M. New insight on carbonisation and graphitisation mechanisms as obtained from a bottom-up analytical approach of X-ray diffraction patterns. *Carbon* **2019**, *147*, 602–611.
- (16) Burian, A.; Dore, J. C.; Hannon, A. C.; Honkimaki, V. Complementary studies of structural characteristics for carbon materials with X-rays and neutrons. *J. Alloys Compd.* **2005**, *401*, 18–23.
- (17) Prem, M.; Krexner, G.; Peterlik, H. Structural investigation of carbon/carbon composites by neutron scattering. *Phys. B* **2006**, *385–386*, 538–541.
- (18) Weisbecker, P.; Leyssale, J.-M.; Fischer, H. E.; Honkimäki, V.; Lalanne, M.; Vignoles, G. L. Microstructure of pyrocarbons from pair distribution function analysis using neutron diffraction. *Carbon* **2012**, *50*, 1563–1573.
- (19) Farbos, B.; Weisbecker, P.; Fischer, H. E.; Da Costa, J.-P.; Lalanne, M.; Chollon, G.; Germain, C.; Vignoles, G. L.; Leyssale, J.-M. Nanoscale structure and texture of highly anisotropic pyrocarbons revisited with transmission electron microscopy, image processing, neutron diffraction and atomistic modeling. *Carbon* **2014**, *80*, 472–489.
- (20) Woznica, N.; Hawelek, L.; Fischer, H. E.; Bobrinetskiy, I.; Burian, A. The atomic scale structure of graphene powder studied by neutron and X-ray diffraction. *J. Appl. Crystallogr.* **2015**, *48*, 1429–1436.
- (21) Jurkiewicz, K.; Duber, S.; Fischer, H. E.; Burian, A. Modelling of glass-like carbon structure and its experimental verification by neutron and X-ray diffraction. *J. Appl. Crystallogr.* **2017**, *50*, 36–48.
- (22) Sears, V. F. Neutron scattering lengths and cross sections. *Neutron News* **1992**, *3*, 26–37.
- (23) Hoffmann, J.-U.; Reehuis, M. E2: The Flat-Cone Diffractometer at BER II. *J. Large Scale Res. Facil.* **2018**, *4*, A129.
- (24) Franz, A.; Hoser, A. E9: The Fine Resolution Powder Diffractometer (FIREPOD) at BER II. *J. Large Scale Res. Facil.* **2017**, *3*, A103.
- (25) Basham, M.; Filik, J.; Wharmby, M. T.; Chang, P. C. Y.; El Kassaby, B.; Gerring, M.; Aishima, J.; Levik, K.; Pulford, B. C. A.; Sikharulidze, I.; et al. Data Analysis WorkbeNch(DAWN). *J. Synchrotron Radiat.* **2015**, *22*, 853–858.
- (26) Filik, J.; Ashton, A. W.; Chang, P. C. Y.; Chater, P. A.; Day, S. J.; Drakopoulos, M.; Gerring, M. W.; Hart, M. L.; Magdysuk, O. V.; Michalik, S.; et al. Processing two-dimensional X-ray diffraction and small-angle scattering data in DAWN 2. *J. Appl. Crystallogr.* **2017**, *50*, 959–966.
- (27) Juhás, P.; Davis, T.; Farrow, C. L.; Billinge, S. J. L. PDFgetX3: a rapid and highly automatable program for processing powder diffraction data into total scattering pair distribution functions. *J. Appl. Crystallogr.* **2013**, *46*, 560–566.
- (28) Farrow, C. L.; Juhas, P.; Liu, J. W.; Bryndin, D.; Božin, E. S.; Bloch, J.; Proffen, T.; Billinge, S. J. L. PDFfit2 and PDFgui: computer programs for studying nanostructure in crystals. *J. Phys.: Condens. Matter* **2007**, *19*, 335219.
- (29) Poulin, A.; Dupont, C.; Martinez, P.; Guizani, C.; Drnec, J. Wide-angle X-ray scattering combined with pair distribution function analysis of pyrolyzed wood. *J. Appl. Crystallogr.* **2019**, *52*, 60–71.
- (30) Farrow, C. L.; Juhas, P.; Liu, J. W.; Bryndin, D.; Božin, E. S.; Bloch, J.; Proffen, T.; Billinge, S. J. L. *PDFgui User Guide*; Board of Trustees of Columbia University, 2016.
- (31) Loeh, M. O.; Badaczewski, F.; Faber, K.; Hintner, S.; Bertino, M. F.; Mueller, P.; Metz, J.; Smarsly, B. M. Analysis of thermally induced changes in the structure of coal tar pitches by an advanced evaluation method of X-ray scattering data. *Carbon* **2016**, *109*, 823–835.